Supporting Information

A bifunctional electrolyte for activating Mg-Li hybrid batteries

Wenlu Sun,†[a] Lu Chen,†[a] Jun Wang,†[a] Hui Zhang,[b] Zhilong Quan,[a] Fang Fu,[a] Huabin Kong,[a] Shibin Wang*[a] and Hongwei Chen*[a, c]

[a] College of Materials Science and Engineering, Huaqiao University, Xiamen 361021, P. R. China.

[b] National Key Laboratory of High-efficiency Utilization of Coal and Green Chemical Engineering, Ningxia University, Yinchuan 750021, P. R. China.

[c] Xiamen Key Laboratory of Optoelectronic Materials and Advanced Manufacturing, College of Materials Science and Engineering, Huaqiao University, Xiamen 361021, P. R. China.

Corresponding Author

*Shibin Wang, E-mail: sbwang@hqu.edu.cn

*Hongwei Chen, E-mail: hwchen@hqu.edu.cn

[†] These authors contributed equally to this work.

Chemicals and materials:

Carboxylated MWCNTs were purchased from XFnano Materials Tech Co., Ltd., China. 1,3,5-benzenetricarboxaldehyde was obtained from Shanghai Tengqian Biotechnology Co., Ltd. $Mg(HDMS)_2$, and LiTFSI was purchased from Sigma-Aldrich. Super P, PVDF, and Cabon Paper were purchased from Shenzhen Kejing Star Technology Co. Melamine, anhydrous dimethyl sulfoxide, Magnesium foil, and other solvents/reagents were all purchased from Aladdin industrial corporation, Shanghai, China., unless otherwise mentioned.

Supplemental results and discussion

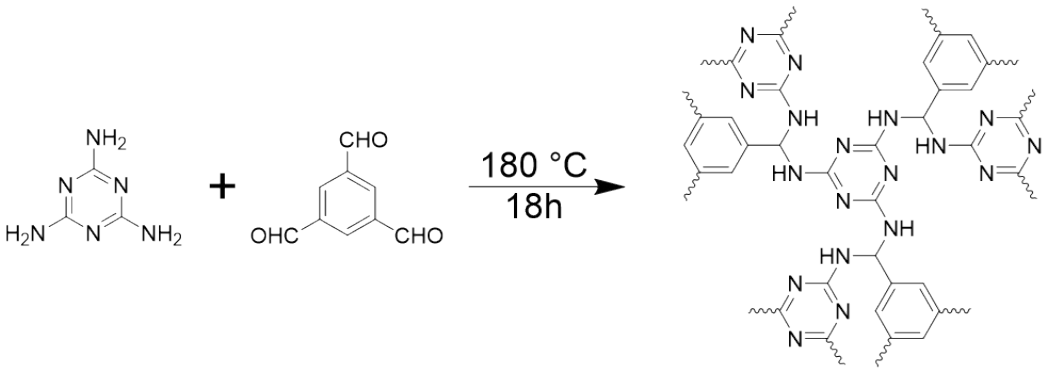

Figure S1. Schematic of the condensation reaction to synthesize POF.[S1]

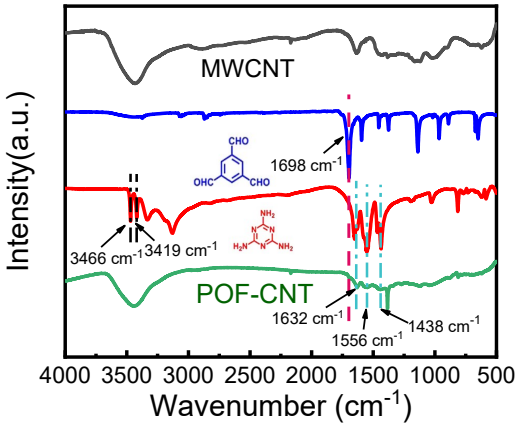

Figure S2. FTIR measurement of the condensation of synthesis POF. For POF on CNT, the stretching vibration of -NH_2 (3466 and 3419 cm^{-1}) from melamine and the stretching vibration of the aldehyde group (1698 cm^{-1}) disappear, Meanwhile, the characteristic bands of quadrant (1556 cm^{-1}) and semicircle (1438 cm^{-1}) stretching of the triazine ring prove that the polycondensation is successful.

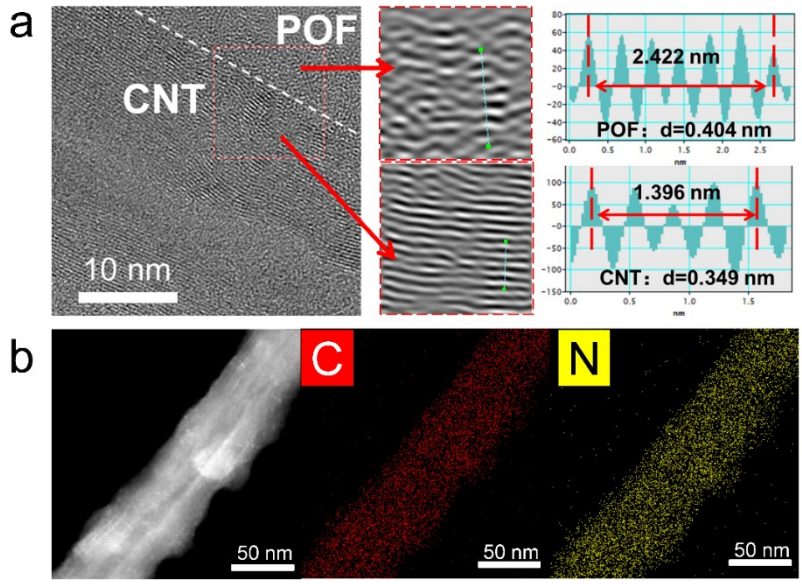

Figure S3. (a) TEM images and lattice fringes and (b) EDX mapping of POF on CNT. In order to exactly calculate the d values at different regions, more than four lattice fringes were measured. The d value of POF is measured to be 0.404 nm, indicating loosely layered-stacking structure compared to CNT with d value of 0.349 nm.

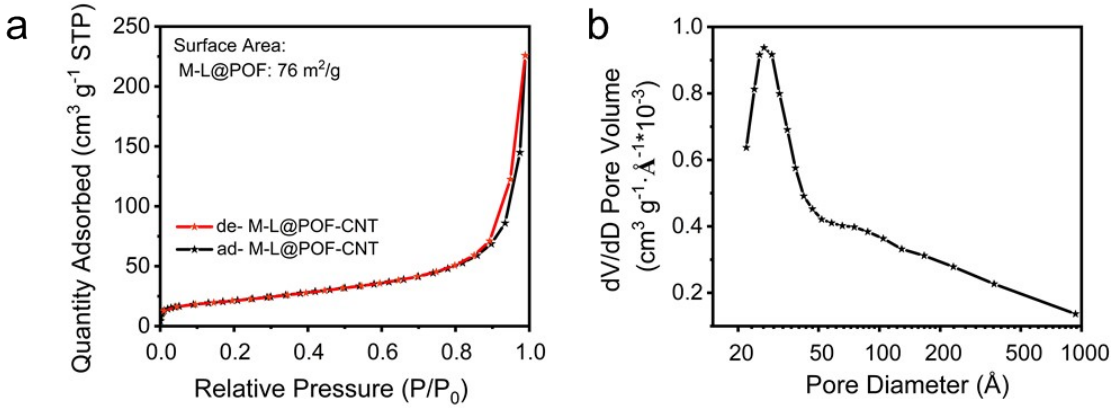

Figure S4. (a) BET surface and (b) pore distribution of POF.

Table S1. The BET results of POF.

BET Surface Area	75.9 m²/g
BJH Pore Volume	0.344 cm³/g
BJH Adsorption average pore diameter	204 Å
BJH Desorption average pore diameter	194 Å

Table S2. Comparison of typical cathode performances in MIBs.

Materials	Capacity / mAh g^{-1}	Voltage platform / V vs. Mg/Mg^{2+}	Cycle number	Current density /mA g^{-1}	Ref.
TiS_2 nanotubes	184	~0.98	80	10	S2
VO_2 (B)	143	2.17	60	100	S3
$H_2V_3O_8$	132	~1.9	100	40	S4
GO/V_2O_5	140	~1.5	20	20	S5
$V_2O_5•nH_2O$@rGO	~97	~2.1	200	1000	S6
MoS_2/C microspheres	119	1.4	20	50	S7
MoS_2/rGO	74	1.4	50	20	S8
$Cu_xMo_6S_8$ ($x \geqslant 1$)	108	~1.0	50	6	S9
$Mg_{0.3}V_2O_5•1.1H_2O$	~90	~2.1	10,000	2000	S10
$Mg_{0.21}Ti_3C_2T_x$	~50	1.5	60	100	S11
$Mo_6S_{8-y}Se_y$	~90	~1.1	100	100	S12
Birnessite MnO_2	183	2.8	30	100	S13
V_2O_5-PEO	96	~1.6	35	10	S14
PVP-MoS_2	132	~0.7	100	20	S15
$Ti_3C_2T_x$/CTAB	135	0.9	250	200	S16
Expanded TiS_2	~120	~0.5	400	240	S17
Amorphous V_2O_5	~130	2.2	40	50	S18
CTF	~114	1.35	3000	570	S18
Mg-P4AQ	130	1.37	100	130	S20
M-L@POF	**221**	~0.5 V	**3000 (83 % retention)**	**360**	**This work**

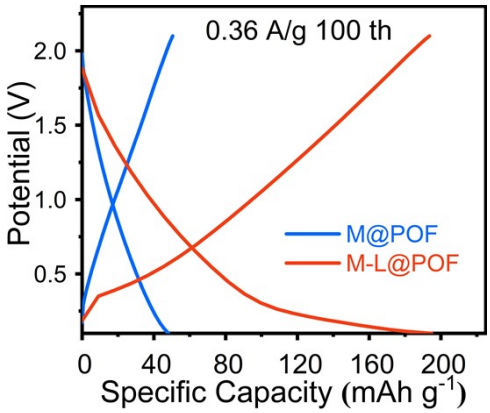

Figure S5. The 100th cycle galvanostatic charge and discharge curves of the M@POF and M-L@POF with current density of 0.36 A/g.

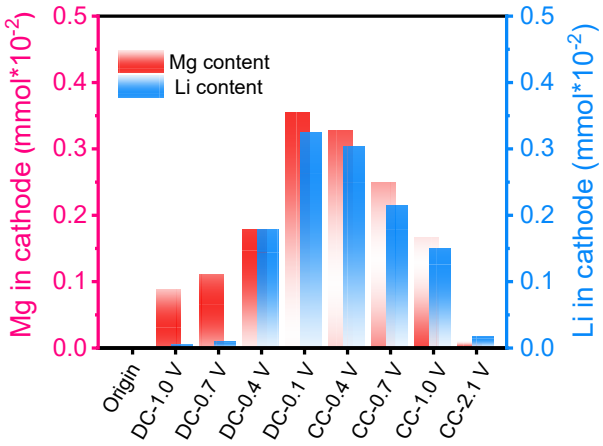

Figure S6. Mg/Li contents of the M-L@POF cathode at different charge/discharge stages of the 100th cycle. (CC: constant current charge, DC: constant current discharge)

Table S3. Calculation of capacity contribution of Mg/Li species.

	Potential vs. Mg^{2+}/Mg V	**Dual-salt electrolyte**		**Mg electrolyte**
		Mg capacity contribution mAh/g	Li capacity contribution mAh/g	Mg capacity mAh/g
Discharge	1.0	**60.0**	**1.5**	16.7
	0.7	**92.1**	**3.6**	24.5
	0.4	**91.3**	**45.4**	34.1
	0.1	**244.9**	**111.4**	48.2
Charge	0.4	**70.6**	**24.9**	3.0
	0.7	**104.0**	**59.7**	10.2
	1.0	**151.7**	**59.7**	18.5
	2.1	**248.6**	**105.4**	50.5

Note S1. The calculation of the actual contribution of magnesium ions and lithium ions in the electrode material was conducted based on the ICP results (Figure S6) and GCD profiles. The amount of relative balance charge is calculated from the Mg:Li atomic ratio, thereby calculating the contribution of the corresponding element in the specific capacity. See the formulas below and Table S3 for details.

$$2 * P_{Mg} * C = C_{Mg}$$

$$P_{Li} * C = C_{Li}$$

$$C_{Mg} + C_{Li} = C$$

The C means corresponding charge and discharge capacity. The P_{Mg} *and* P_{Li} represent the proportion of working ions (Mg and Li) to the total working ions in cathode at the corresponding working potential. The charge transfer amount for Mg ion is considered as double electron transfer and Li ion as single electron transfer.

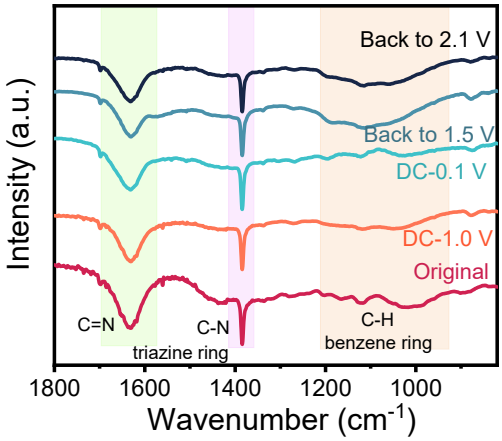

Figure S7. *Ex-situ* FTIR measurement of the discharged M-L@POF electrode.

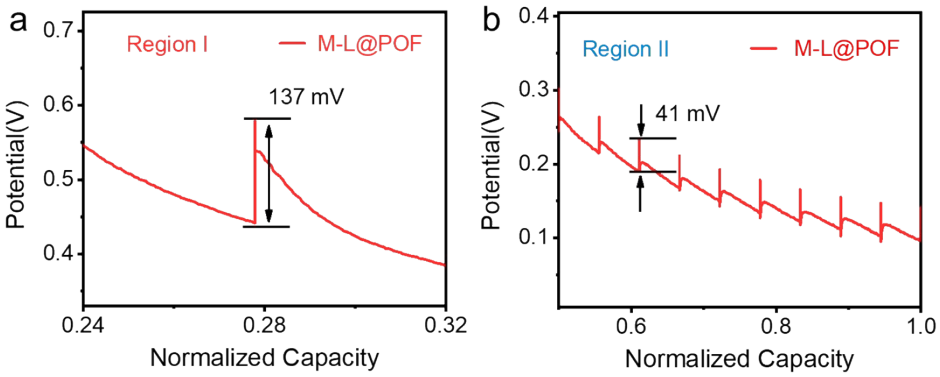

Figure S8. The enlarged graph of overpotential in Region I (a) and Region II (b) with M-L@POF.

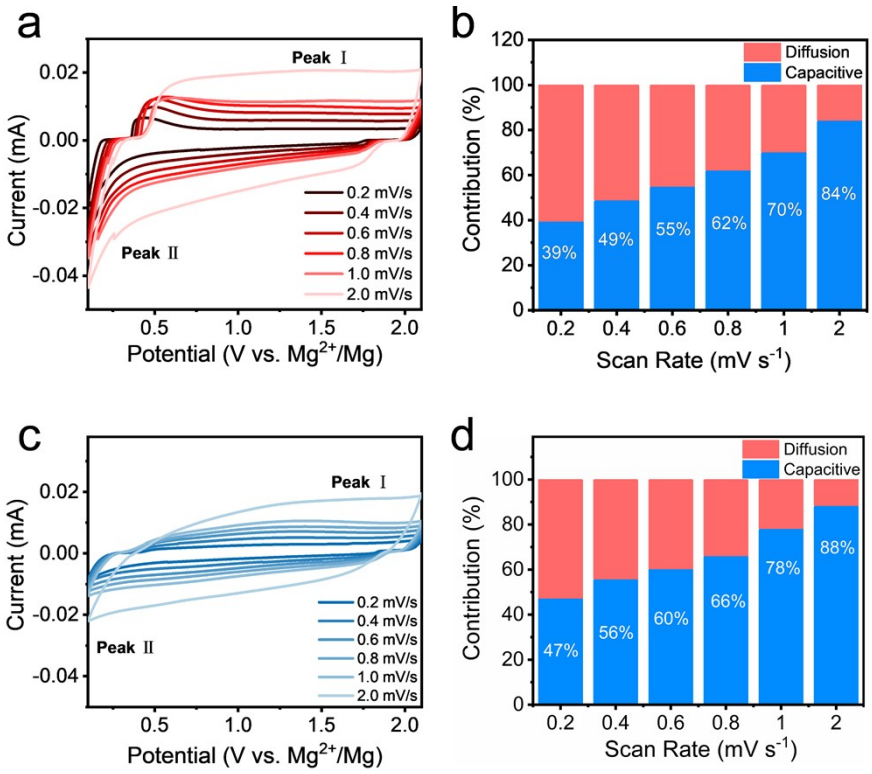

Figure S9. CV curves of M-L@POF and M@POF at different sweep rates (a) and (c) respectively, (b) and (d) refer to the corresponding capacity contribution. Calculation of the b value also was taken value from the corresponding peak current respectively. The Peak I and Peak II correspond to the peak position of the positive sweep and the peak position of the negative sweep.

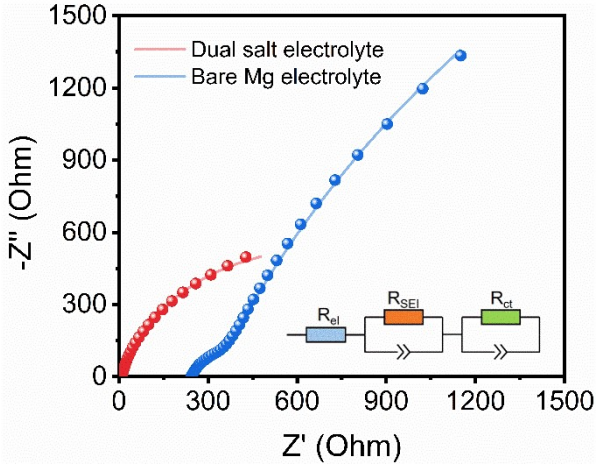

Figure S10. EIS measurement of Mg//Mg cells with different electrolytes.

The interfacial resistance in Mg//Mg cells was calculated according to *Nat Mater. 2017* 16(5): 572-579. The total impedances are ~1322 and 8190 Ω cm^2 for the cells cycled in Mg-Li electrolyte and Mg electrolyte, respectively. The ion conductivities of electrolytes were measured via two stainless steel electrodes separated by polytetrafluorethylene (PTFE) film, with EIS technology tested between 0.1 Hz to 1 MHz. The obtained electrolyte resistances are ~1.4 Ω cm^2 for dual salt electrolyte and ~230 Ω cm^2 for bare Mg electrolyte. According to these data, the interface resistance is equal to the total impedance minus the bulk electrolyte impedance, then divided by two. The final interface resistance is ~660 and 3980 Ω cm^2 for the cells cycled in dual salt and bare Mg electrolyte, respectively.

Table S4. The calculated interfacial resistance

	Bulk electrolyte Resistance (Ω cm^2)	**Total Resistance (Ω cm^2)**	**Interface Resistance (Ω cm^2)**
Dual salt electrolyte	1.4	1322	660
Bare Mg electrolyte	230	8190	3980

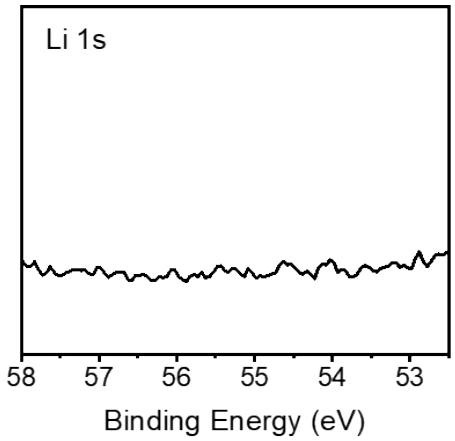

Figure S11. XPS Li1s spectra of the Mg foil after 200 h cycled in dual-salt electrolyte. No Li electrodeposited on the surface of Mg foil.

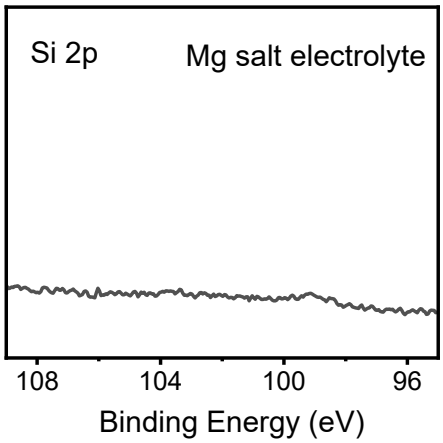

Figure S12. XPS Si2p spectra of the Mg metals operated 200 h cycled in bare Mg salt electrolyte. No obvious signal of organic-silicon component Si2p can be found.

Table S5. Calculations of actual cell energy density.

	Cathode Active Material Mass Loading	Cathode Areal Mass Loading	Practical Cathode Area Capacity	Cathode Active Material special Capacity	Cathode Active Material special energy	Anode Area Mass Loading	Electrolyte Density	Electrolyte area mass	Total area mass	Total energy area output	Actual energy density
	mg cm^{-2}	mg cm^{-2}	mAh cm^{-2}	mAh g^{-1}	Wh kg^{-1}	mg cm^{-2}	g cm^{-3}	mg cm^{-2}	mg cm^{-2}	mWh cm^{-2}	Wh kg^{-1}
M-L@POF (This work)	1.05	1.50	0.37	354.25	161.48	0.17	1.10	5.78	**7.44**	169.55	**22.78**
M@POF (This work)	1.05	1.50	0.07	63.09	52.31	0.17	1.00	5.25	**6.92**	54.93	**7.94**
M@POF coupled with dual salt electrolyte	1.05	1.50	0.07	63.09	52.31	0.17	1.10	5.78	**7.44**	54.93	**7.38**
CTF [S19]	1.05	1.50	0.12	114.00	153.90	0.05	1.20	6.30	**7.85**	161.60	**20.57**
PHV-Cl [S22]	1.05 (estimated)	3.00	0.18	171.00	222.30	0.08	1.30	6.83	**9.91**	233.42	**23.56**
Mg-P14AQ [S20]	1.00	2.50	0.19	193.00	265.38	0.09	1.10	5.50	**8.09**	265.38	**32.81**
Mo_6S_8 [S23]	3.92	4.90	0.31	80.00	108.00	0.14	1.30	25.48	**30.52**	423.36	**13.87**

*CTF, PHV-Cl, Mg-P14AQ, and Mo_6S_8 were used as Mg cathodes.

Note S2. The calculation of energy density takes into account the mass of the cathode (active materials + conductive addictive + binder), anode, and electrolyte (solvent + salt). The theory specific capacity of Mg was regarded as 2205 mAh g^{-1}. The amount of electrolytes addition are set to 5 uL/$mg_{active\text{-}material}$, referring to the theoretical amount of NCA vs. Li to reflect the idealized actual application situation, rather than just calculating the active materials or only considering the salt. The calculation was conducted partially referenced to *Adv. Energy Mater. 2019*, 9, 1803170.

$$Energy\ Output_{total} = Mass_{active\ materials} \times Energy\ Density_{active\ materials}$$

$$Mass_{total} = Mass_{cathode} + Mass_{anode} + Mass_{electrolyte}$$

$$Energy\ Density_{over\ all} = Energy\ Output_{total} \div Mass_{total}$$

References

S1. Liu, L.; Li, P.-Z.; Zhu, L.; Zou, R.; Zhao, Y. Polymer 54 (2013) 596-600.

S2. Z. Tao, L. Xu, X. Gou, J. Chen, H, Yuan, Chem. Commun. 40 (2004) 2080–2081.

S3. T. Luo, Y. Liu, H. Su, R. Xiao, L. Huang, Q. Xiang, Y. Zhou, C. Chen, Electrochim. Acta 260 (2018) 805–813

S4. M. Rastgoo-Deylami, M.S. Chae, S. Hong, Chem. Mater. 30 (2018) 7464–7472.

S5. X. Du, G. Huang, Y. Qin, L. Wang, RSC Adv. 5 (2015) 76352–76355.

S6. Q. An, Y. Li, H. Deog Yoo, S. Chen, Q. Ru, L. Mai, Y. Yao, Graphene decorated vanadium oxide nanowire aerogel for long-cycle-life magnesium battery cathodes, Nano Energy 18 (2015) 265–272

S7. Y. Liu, L. Jiao, Q. Wu, J. Du, Y. Zhao, Y. Si, Y. Wang, H. Yuan , J. Mater. Chem. A 1 (19) (2013) 5822.

S8. Y. Liu, L. Jiao, Q. Wu, Y. Zhao, K. Cao, H. Liu, Y. Wang, H. Yuan, Nanoscale 5 (20) (2013) 9562.

S9. S.-G. Woo, J.-Y. Yoo, W. Cho, M.-S. Park, K.J. Kim, J.-H. Kim, J.-S. Kim, Y.-J. Kim, RSC Adv. 4 (103) (2014) 59048–59055

S10. Y. Xu, X. Deng, Q. Li, G. Zhang, F. Xiong, S. Tan, Q. Wei, J. Lu, J. Li, Q. An, L. Mai, Chem 5 (5) (2019) 1194–1209.

S11. M. Zhao, C.E. Ren, M. Alhabeb, B. Anasori, M.W. Barsoum, Y. Gogotsi , ACS Appl. Energy Mater. 2 (2019) 1572–1578.

S12. E. Levi, E. Lancry, A. Mitelman, D. Aurbach, G. Ceder, D. Morgan, O. Isnard, Chem. Mater. 18(2006) 5492-5503.

S13. K.W. Nam, S. Kim, S. Lee, M. Salama, I. Shterenberg, Y. Gofer, J. Kim, E. Yang, C. S. Park, J. Kim, S. Lee, W. Chang, S. Doo, Y.N. Jo, Y. Jung, D. Aurbach, J.W. Choi, Nano Lett. 15 (2015) 4071–4079.

S14. S.D. Perera, R.B. Archer, C.A. Damin, R. Mendoza-Cruz, C.P. Rhodes, J. Power Sources 343 (2017) 580–591.

S15. C. Wu, G. Zhao, S. Gong, N. Zhang, K. Sun, J. Mater. Chem. A 7 (2019) 4426–4430.

S16. M. Xu, S. Lei, J. Qi, Q. Dou, L. Liu, Y. Lu, Q. Huang, S. Shi, X. Yan, ACS Nano 12 (4) (2018) 3733–3740.

S17. H.D. Yoo, Y. Liang, H. Dong, J. Lin, H. Wang, Y. Liu, L. Ma, T. Wu, Y. Li, Q. Ru, Y. Jing, Q. An, W. Zhou, J. Guo, J. Lu, S.T. Pantelides, X. Qian, Y. Yao, Nat. Commun. 8 (2017) 339.

S18. Z. Wei, D. Wang, X. Yang, C. Wang, G. Chen, F. Du, Adv. Mater. Interfaces 5 (2018) 1800639

S19. R. Sun, S. Hou, C. Luo, X. Ji, L. Wang, L. Mai, C. Wang, Nano Lett. 20 (2020) 3880.

S20. H. Dong, Y. Liang, O. Tutusaus, R. Mohtadi, Y. Zhang, F. Hao, Y. Yao, Joule 3 (2019) 782.

S21. Betz, J.; Bieker, G.; Meister, P.; Placke, T.; Winter, M.; Schmuch, R. Adv. Energy Mater. 9 (2019) 1803170.

S22. Ikhe, A. B.; Naveen, N.; Sohn, K.-S.; Pyo, M. Electrochim. Acta 283 (2018) 393−400.

S23.Saha, P.; Jampani, P. H.; Datta, M. K.; Okoli, C. U.; Manivannan, A.; Kumta, P. N. J. Electrochem. Soc. 161 (2014) A593−A598.